Machine-learning-assisted classification of construction and demolition waste fragments using computer vision: convolution versus extraction of selected features

V. Nežerka[a,*], T. Zbíral[a], J. Trejbal[a]

[a]*Faculty of Civil Engineering, Czech Technical University in Prague, Thákurova 7, 166 29 Praha 6, Czech Republic*

Abstract

Improper sorting of construction and demolition waste (CDW) leads to significant environmental and economic implications, including inefficient resource use and missed recycling opportunities. To address this, we developed a machine-learning-assisted procedure for recognizing CDW fragments using an RGB camera. Our approach uniquely leverages selected feature extraction, enhancing classification speed and accuracy. We employed three classifiers: convolutional neural network (CNN), gradient boosting (GB) decision trees, and multi-layer perception (MLP). Notably, our method's extraction of selected features for GB and MLP outperformed the traditional CNN in terms of speed and accuracy, especially for challenging samples with similar textures. Specifically, while convolution resulted in an overall accuracy of 85.9%, our innovative feature extraction approach yielded accuracies up to 92.3%. This study's findings have significant implications for the future of CDW management, offering a pathway for efficient and accurate waste sorting, fostering sustainable resource use, and reducing the environmental impact of CDW disposal. Supplementary materials, including datasets, codes, and models, are provided, promoting transparency and reproducibility.

Keywords: CDW management, Image-based sorting, Texture analysis, Algorithm evaluation, Automated classification

*Corresponding author

Email addresses: vaclav.nezerka@cvut.cz (V. Nežerka), zbiratom@student.cvut.cz (T. Zbíral), jan.trejbal@fsv.cvut.cz (J. Trejbal)

Abbreviations

CDW	Construction and demolition waste
AAC	Autoclaved aerated concrete
GB	Gradient boosting
MLP	Multi-layer perception
CNN	Convolutional neural network
SVM	Support vector machine

1. Introduction

The construction industry has a significant socio-economic role as it generates around 25% of the global GDP and employs 7% of the population (Norouzi et al., 2021). In the EU, 18 mil. people were employed in the construction sector in 2020 (Benachio et al., 2020). However, the sector is responsible for the enormous consumption of raw materials and large production of waste. Globally, it is estimated that the construction industry consumes over 30–40% of all natural resources extracted (Darko et al., 2020; Purchase et al., 2021), generates around 25–40% of the total solid waste (Nasir et al., 2017), and emits up to 25% of anthropogenic CO_2 (Mahpour, 2018). In 2020, the production of construction and demolition waste (CDW) in the EU was estimated to be around 747.3 mil. tons, which amounts to approximately 1685 kg per capita[1].

In order to pursue sustainable development, it is imperative to manage waste in a prudent and cost-effective manner and adopt the principles of circular economy (Joensuu et al., 2020; Oluleye et al., 2022). Following this direction, the European Parliament and the Commission issued Directive No 98/2008 which required the EU member states to increase the overall recycling of waste to at least 70% by weight from 2020. Even though the rate of CDW recycling in the EU is almost constant, at about 90% on average[2], the lion's share is downcycled. At the global scale, rapidly developing countries, such as China with 2 bn tons/year, are even bigger CDW producers

[1] https://ec.europa.eu/eurostat/databrowser/view/env_wasgen/default/bar
[2] https://ec.europa.eu/eurostat/databrowser/view/cei_wm040/default/table

than all the EU states combined (Zheng et al., 2017).

The most commonly recycled CDW materials, besides soils, are concrete and ceramics, mostly used for embankments, backfills, fillings, or beddings under foundation slabs or pavings. Less frequently, the recycled fragments are used as aggregates in the production of new concrete mixes or the finest fractions as micro-fillers (Hlůžek et al., 2020; Prošek et al., 2020; Valentin et al., 2021; Nežerka et al., 2023). The major limiting factor in the crushed CDW valorization in applications such as concrete manufacturing is improper sorting (Hoong et al., 2020). Su (2020) carried out a multi-agent evolutionary game study and concluded that research into CDW classification holds the greatest potential to promote CDW recycling and reuse. Davis et al. (2021) pointed out that the automatic classification of CDW materials would significantly reduce the costs associated with sorting.

At the pre-sorting stage, methods exploiting gravitational, magnetic, inertial, electrostatic, or buoyancy forces are very efficient in separating specific types of materials from a heterogeneous CDW mix (Gundupalli et al., 2017; Vincent et al., 2022). Leveraging big data in CDW management offers promising advancements. Yuan et al. (2021) utilized a dataset of 4.27 million truckloads of construction waste to estimate waste composition based on bulk density. Such techniques can significantly refine sorting processes and promote sustainable resource utilization.

Despite recent progress in advanced methods based on research into the development of various sensors (image, spectroscopic, spectral, UV sensitive, etc.) (Gundupalli et al., 2017; Lu and Chen, 2022), sorting of the remaining fragments is at the industrial scale most commonly accomplished manually and cannot be done properly due to their similarity. Therefore, it is desirable to replace manual sorting with robotic vision-based technologies such as RGB cameras, hyperspectral imaging, or X-ray sensors assisted with machine learning. This approach has been first employed for the purpose of municipal waste separation (Özkan et al., 2015; Wang et al., 2019b; Liang and Gu, 2021; Lu and Chen, 2022) and the extensive development led to the sorting accuracy exceeding 90% (Yang et al., 2021).

The robotic vision-based technology has also started to find its way into the CDW sorting (Wang et al., 2019a, 2020). However, automatic CDW recognition encountered its limitations in terms of

accuracy and boundary identification. The latter issue was addressed by Dong et al. (2022), who proposed a boundary-aware model with the ability to distinguish and segment individual materials within structural debris. Convolutional Neural Networks (CNNs) are specialized for image recognition, leveraging their ability to identify hierarchical patterns in visual data. Their design enables them to dissect images into components, enhancing classification accuracy, especially in intricate tasks like CDW sorting. For instance, Xiao et al. (2020) utilized CNNs to effectively classify different CDW materials, underscoring the potential of this approach in the domain. They classified different CDW materials (wood, brick, rubber, rock, concrete) with an accuracy exceeding 80%. Ku et al. (2020) built a robotic line that automatically recognized and classified the basic materials within CDW using hyperspectral and 3D cameras with an accuracy of about 90%. Machine-learning classification was also employed by Lin et al. (2022), who recognized visually different CDW fragments and achieved an accuracy ranging between 75 and 80%. The closest to our goal is the study by Hoong et al. (2020), who employed neural networks for the classification of recycled aggregates. They constructed a library of 36,000 images of individual aggregate grains and their model achieved accuracies of up to 97%.

While previous studies have employed CNN-based models for CDW classification, our research distinguishes itself in two primary ways. Firstly, we focus on the efficient extraction of features describing the textures captured using ordinary RGB cameras, a method not extensively explored in prior work. Secondly, we provide a comprehensive comparison between CNN and other machine-learning models, specifically gradient boosting (GB) and multi-layer perception (MLP), showcasing the efficacy of feature extraction in enhancing both speed and accuracy. This paper presents a unique approach to CDW fragment recognition, emphasizing the power of feature extraction. We provide extensive datasets, computer codes, and pre-trained models, ensuring our methodology is transparent, reproducible, and can be built upon by other researchers or industry stakeholders.

2. Methodology

The capabilities and limitations of the selected feature extraction methods and machine-learning models are demonstrated on four types of CDW fragments. These were chosen because they are

the most common fragments found in mixed debris from demolition sites in the Czech Republic: light-colored aerated autoclaved concrete (AAC), asphalt conglomerates, ceramics (roof tiles and bricks), and concrete. These materials not only represent a significant portion of the total waste but also pose a challenge in terms of their similarity, making their accurate classification crucial for efficient recycling and waste management.

2.1. Collection of datasets

The 1920×1280 px images of ∼30–250mm fragments were taken from a distance of about 70 cm using a handheld digital single-lens reflex camera (Canon EOS 70D with a Canon zoom lens EF-S 17-85 IS USM) in a CDW collection and sorting yard near Kladno, Czech Republic (Figure 1). The images were captured in a shade to minimize variations in illumination and to ensure consistent image quality. Importantly, the CDW fragments were used in their natural state from the yard, without any presorting or cleaning, reflecting the real-world conditions of such waste. In a potential industrial deployment, techniques like air-flow cleaning could be introduced on conveyor belts to minimize dirt and dust, enhancing the image clarity. The fragments were placed on the ground while taking the images, or directly on the CDW piles.

Unlike clean structural elements, whose classification has been tackled in other studies (Zhu and Brilakis, 2010; Son et al., 2012; Dimitrov and Golparvar-Fard, 2014; Han and Golparvar-Fard, 2015; Braun and Borrmann, 2019; Mahami et al., 2020), recognition of CDW fragments is a more challenging task as their surface can be contaminated with dust and residues of other materials. Randomly selected samples of CDW fragments are presented in Figure 2, showing similar textures, especially in the case of AAC and concrete. The complete image datasets used for training of machine-learning classifiers and validation are open and provided as supplementary material (Nežerka et al., 2023).

The acquired image datasets were manually split to individual material classes. The annotated images within each class were divided into training and testing sets in a 4:1 ratio. Since the shape of fragments cannot be the key for classification and the classifiers were trained to recognize the CDW textures, 200×200 px regions (image subsets) were manually extracted for training and testing of the selected classifiers (Figure 3). The summary of these training/testing data is provided

Figure 1: The site for collecting images, a CDW collection and sorting yard near Kladno, Czech Republic.

Figure 2: Examples of image datasets for the examined CDW materials.

in Table 1.

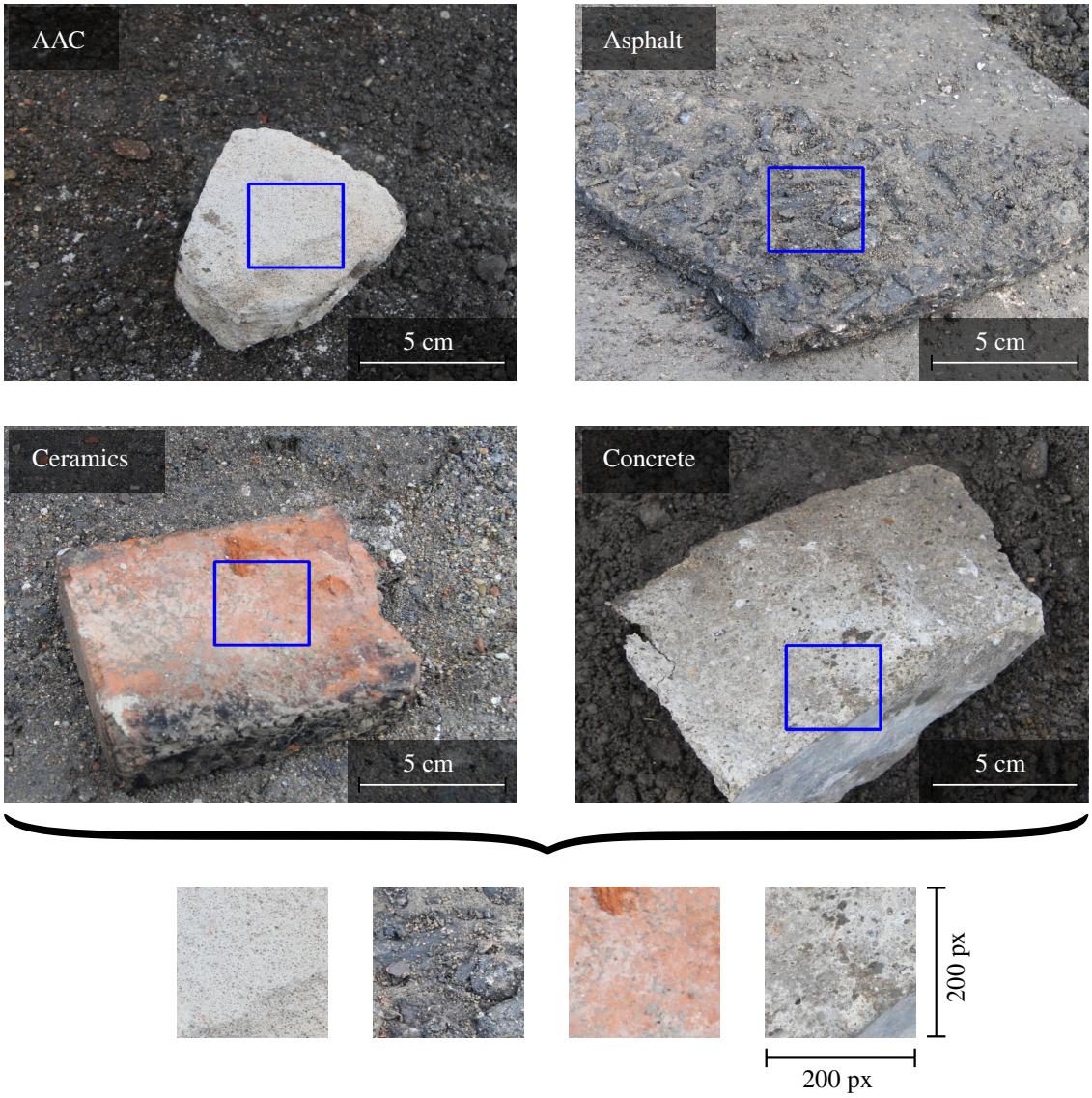

Figure 3: Manual extraction of 200×200 px regions (image subsets) used for training and testing of selected classifiers.

2.2. *Extraction of features*

Images represent a high-dimensional input space with $D = N \times N \times C$ features, where $N \times N$ is the image subset size (px) and C is the number of color channels (equal to 3). Such large inputs can be tackled using CNNs, yet reducing the input space by extracting informative numeric features that describe the CDW texture (Figure 4) allows to use simple and efficient classification

Table 1: Summary of extracted 200×200 px image subsets used for testing and training of selected classifiers.

Material (class)	Number of training images	Number of testing images
AAC	939	235
Asphalt	902	226
Ceramics	620	155
Concrete	825	206

algorithms. In this study, we scrutinize the gradient boosting (GB) and multi-layer perception (MLP) models for such a classification based on extracted features.

The following metrics are proposed to describe the color and texture of CDW fragments, reducing the input space to $D = 4$: (i) mean intensity, (ii) mean intensity of a selected color channel, (iii) Shannon entropy, and (iv) mean intensity gradient. To calculate these quantities, local coordinates (i, j) are introduced for image subsets (Figure 5). The 3-dimensional matrix of intensities for individual color channels, $I(C, i, j)$, was reduced to a single-channel matrix $I(1, i, j) \equiv I_{\mathrm{gray}}(i, j)$, representing a gray-scale image, as

$$I_{\mathrm{gray}}(i,j) = 0.299\, I_{\mathrm{red}}(i,j) + 0.587\, I_{\mathrm{green}}(i,j) + 0.114\, I_{\mathrm{blue}}(i,j), \tag{1}$$

where $I_{\mathrm{red}}(i, j)$, $I_{\mathrm{green}}(i, j)$, and $I_{\mathrm{blue}}(i, j)$ represent the matrices of intensities for the red, green, and blue channel, respectively. The weights for individual channels follow luma encoding that reflects different human vision sensitivity to particular colors.

2.2.1. Mean intensity

Mean intensity, $\overline{I_{\mathrm{gray}}}$, is strongly influenced by the illumination of a captured scene and cannot be considered a reliable feature if constant illumination is not ensured for all (training, testing, and classified) images. Since this proof-of-the-concept study is intended as a cookbook for CDW fragments recognition on conveyor belts in an indoor environment, $\overline{I_{\mathrm{gray}}}$ can be considered as one of the relevant features for classification and is calculated as

$$\overline{I_{\mathrm{gray}}} = \sum_{i=1}^{N} \sum_{j=1}^{N} \frac{I_{\mathrm{gray}}(i,j)}{N^2}. \tag{2}$$

Figure 4: Visualization of the image subset characteristics for individual materials (classes) as pairwise scatter plots; marginal distributions of each feature for each class are plotted on the diagonal.

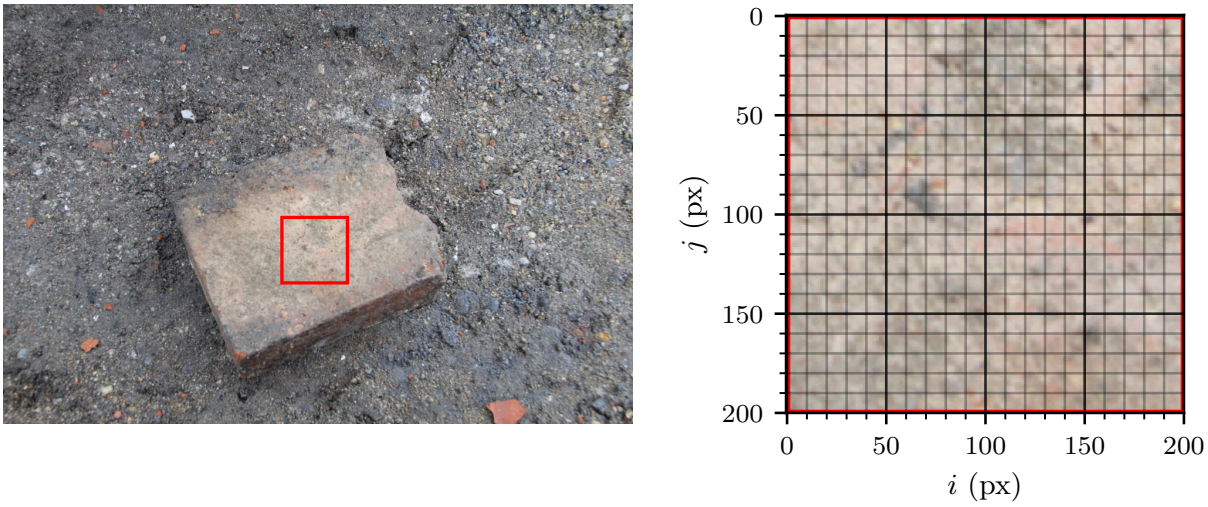

Figure 5: Local coordinates (i, j) for a subset of pixels (right) arbitrarily located within an image of a CDW fragment (left).

2.2.2. *Mean intensity of red color*

The color distribution is one of the key features and many machine-learning models for material recognition were based purely on color-based classification (Son et al., 2012). It was found during a preliminary analysis that for CDW materials, it is sufficient to focus on the predominance of a specific color. Given the orange/reddish color of ceramic fragments, the mean intensity of the red channel, $\overline{I_{\mathrm{red}}}$, relative to the mean intensity (brightness) was selected as the most appropriate color-related label and its value was calculated as

$$\overline{I_{\mathrm{red}}} = \sum_{i=1}^{N} \sum_{j=1}^{N} \frac{I_{\mathrm{red}}(i,j)}{N^2} \frac{1}{\overline{I_{\mathrm{gray}}}}. \tag{3}$$

2.3. *Shannon's entropy*

Many distinct CDW materials have similar colors and color-based labeling may fail (Dimitrov and Golparvar-Fard, 2014; Bosché et al., 2015; Nežerka and Trejbal, 2019). To evaluate the randomness of a texture pattern as an additional feature, Shannon's entropy appears to be the most easy-to-calculate measure (Wu et al., 2013; Antoš et al., 2017; de Sousa Filho et al., 2022). It was first proposed by Claude Shannon in 1948 to evaluate the average level of uncertainty in a signal

as (Shannon, 1948; Wu et al., 2011)

$$H = -\sum_{I_{\text{gray}}=0}^{255} P(I_{\text{gray}}) \log_2 P(I_{\text{gray}}), \tag{4}$$

where $P(I_{\text{gray}}) \in [0, 255]$ (8-bit images) is the frequency of gray pixels' intensity. High values of H indicate higher uncertainty (randomness) of the signal (image).

2.3.1. Mean intensity gradient

Mean intensity gradient ($\overline{\nabla_I}$) was proposed by Pan et al. (2010) as an indicator of stochastic pattern quality in regard to digital image correlation measurements. It evaluates the frequency and intensity of irregularities within an image. Such a measure is directly related to the texture roughness, being another crucial feature used for material classification (Yuan et al., 2020). In this study, the mean intensity gradient was calculated as

$$\overline{\nabla_I} = \sum_{i=1}^{N}\sum_{j=1}^{N} |\nabla I_{\text{gray}}(i,j)| \frac{1}{N^2}, \tag{5}$$

where $|\nabla I_{\text{gray}}(i,j)| = \sqrt{I_i(i,j)^2 + I_j(i,j)^2}$ is the modulus of local intensity gradient and I_i and I_j are the i-directional and j-directional derivatives of $I_{\text{gray}}(i,j)$ at each pixel location (i,j). The differentiation was accomplished using a Sobel operator with a 3×3 kernel (Nixon and Aguado, 2020).

2.4. Classifiers

The machine-learning models used for classification are only briefly introduced in the following sections, along with a presentation of input parameters for each model. Detailed descriptions and analyses of the models are beyond the scope of this paper. The curious reader is referred to comprehensive books on machine learning such as ones by Géron (2022) and Murphy (2022).

The choice of classifiers in this study was driven by the aim to span a spectrum of algorithmic complexity and to capture the strengths of different types of models. Specifically:

1. GB is renowned for its efficiency in classification tasks. It excels in handling structured data and can seamlessly navigate the non-linear relationships between features, making it a robust choice for our dataset (Zhou, 2021).

2. MLP, as a basic form of artificial neural networks (ANNs), bridges the gap between traditional machine learning and deep learning techniques (Ho et al., 2023). Its inclusion allowed us to gauge the efficiency of a simpler neural network architecture in the context of CDW recognition.
3. CNN was incorporated as a benchmark due to its inherent layered analysis capabilities. By automatically extracting features, CNNs detect edges and intricate patterns. Its performance provides insights into how deep learning techniques interpret the visual features in the CDW fragments.

The performance of individual classifiers was tested on a custom-built desktop computer equipped with an Intel 4 core i3-8350K CPU, 16 GB RAM, 250 GB SSD hard drive, Windows 10 operating system, and Python 3.10.9. The Python codes and pre-trained models are provided along with this paper (Zbíral and Nežerka, 2023).

2.4.1. Gradient boosting

GB is a machine learning algorithm that typically uses decision trees (Salzberg, 1994) as its base models (Friedman, 2001). The decision tree is a flowchart-like tree structure where each internal node tests an attribute, and the connected branches represent an outcome of the test. Analogically to leaves, the terminal nodes hold class labels (Friedman, 2002).

At each iteration, GB trains a weak decision tree model on the residual errors between the true and predicted labels of the previous iteration. The final prediction is made by adding up the predictions of all the decision trees, where the contribution of each tree depends on its weight, determined by the improvement in the loss function after adding the tree to the ensemble. The loss function is minimized using gradient descent. The algorithm usually outperforms random forest classifiers in terms of speed and accuracy of the predictions (Hastie et al., 2008; Piryonesi and El-Diraby, 2021).

The GB classifier used in this study was implemented in the Scikit-Learn v.1.1.3 Python package. Standardization of features was performed using the *preprocessing.StandardScaler* class. Cross-validation was accomplished using the *model_selection.StratifiedShuffleSplit* class that provides randomly selected indices to split datasets into test/train data and preserves the percent-

age of samples for each class. The input parameters for the *ensemble.GradientBoostingClassifier* model class were defined as summarized in Table 2. The optimum parameters were selected based on the prediction accuracy and speed. The optimization was done using the Scikit-learn's *model_selection.GridSearchCV* class that provides an exhaustive search over specified values of model parameters (learning rate $\in$ [0.2, 0.8], maximum depth $\in$ [3, 5], and a number of estimators $\in$ [100, 200]). Other input parameters were kept in their default settings.

Table 2: Summary of input parameters for the GB classifier implemented in Scikit-Learn v.1.1.3 (*ensemble.GradientBoostingClassifier* model class).

Input parameter	Keyword argument	Value	Note
Random state	random_state	0	Fixing the random state ensures deterministic behavior during fitting
Learning rate	learning_rate	0.4	Learning rate shrinks the contribution of each tree
Maximum depth	max_depth	4	Maximum depth of individual regression estimators, limiting the number of nodes in decision trees
Number of estimators	n_estimators	125	Number of boosting stages to perform

2.4.2. Multi-layer perception

MLP is a type of artificial neural network that consists of an input layer, a specified number of hidden layers, and an output layer (Rumelhart et al., 1986; Hinton et al., 2006). The input layer represents the features of the input data, while the output layer represents the predicted probability for all classes. The hidden layers are used to learn the non-linear transformations of the input features that lead to the final prediction. In our implementation, the MLP model consists of a single hidden layer; this hidden layer consists of neurons, where each neuron applies a weighted sum of the input features and a bias term, followed by an activation function, such as sigmoid or hyperbolic tangent (tanh). The weights and biases are learned through backpropagation, where the gradients of the loss function are computed to update the weights and biases using gradient descent.

Also, the MLP classifier was implemented in the Scikit-Learn v.1.1.3 Python package. The training procedure was similar to that of the GB model: the standardization of features was

performed using the *preprocessing.StandardScaler* class and *model_selection.StratifiedShuffleSplit* class was used for cross-validation. The input parameters for the *neural_network.MLPClassifier* model class were defined as summarized in Table 3. The search for optimum parameters was also accomplished using the Scikit-learn's *model_selection.GridSearchCV* class, searching over specified values of model parameters (learning rate $\in$ {adaptive, constant $\in$ [0.005, 0.015, 0.05]}, solver $\in$ {stochastic gradient descent, stochastic gradient-based optimizer (adam) (Kingma and Ba, 2015)}, activation $\in$ {rectified linear unit function (ReLU), hyperbolic tan function (tanh)}, and a hidden layer size $\in$ [5, 100]). Other input parameters were kept in their default settings.

Table 3: Summary of input parameters for the MLP classifier implemented in Scikit-Learn v.1.1.3 (*neural_network.MLPClassifier* model class).

Input parameter	Keyword argument	Value	Note
Random state	random_state	0	Fixing the random state ensures deterministic behavior during fitting
Learning rate	learning_rate_init	0.015	Controls the step-size in updating neuron weights
Maximum number of iterations	max_iter	800	Number of epochs (how many times each data point is used)
Learning rate schedule	learning_rate	'constant'	Selected constant learning rate
Solver	solver	'adam'	Weight optimization using the Adam algorithm (Kingma and Ba, 2015)
Neuron activation function	activation	'tanh'	Activation function for the hidden layer
Hidden layer size	hidden_layer_sizes	(20,)	Single hidden layer with 20 neurons

2.4.3. Convolutional neural network

CNN is a type of artificial neural network that is designed for the analysis of data with a grid-like topology (e.g., images) (Zhou et al., 2012; LeCun et al., 2015; Krizhevsky et al., 2017). It consists of several layers, including convolutional layers, pooling layers, and fully connected layers. The convolutional layer applies a convolution operation to the input image, where the convolution kernel slides over the image and computes the dot product between the kernel and the local patch of the image to extract features. The convolutional layer is followed by an activation

function that applies non-linear transformations to the output of the convolution. The pooling layer reduces the spatial dimensions of the output of the convolutional layer by applying a pooling operation, such as max pooling, that takes the maximum value of a local patch. The fully connected layer combines the features learned by the convolutional and pooling layers and makes the final prediction. The weights and biases of the convolutional and the fully connected layers are adjusted during the network training through backpropagation, exploiting the gradient descent algorithm.

Unlike GB and MLP classifiers, CNN takes the whole image as input. Since the model in our study was trained on 200×200 px 3-channel (RGB) images, images for classification having a different size were rescaled to 200×200 px using an interpolation function. The CNN classifier was implemented in the Tensorflow Keras v.2.10.0 Python package, provided by the *models.Sequential* class.

Different architectures of CNNs with various number of filters for the convolutional layers have been tested. The selected model includes three convolutional layers, each followed by a max pooling layer, a flatten layer, and two dense layers. The first and third convolutional layers have 32 3×3 filters, a stride of 1, and a ReLU activation function. The second convolutional layer has 64 3×3 filters and the same activation function. The max pooling layers downsample the feature maps by a factor of two to make the model more efficient. The flatten layer converts the 2D feature maps into a 1D vector. The two dense layers consist of 256 units with a ReLU activation function, followed by an output layer with four neurons corresponding to the individual CDW classes.

The selected model architecture is described in detail in Table 4. During the training process, the model achieved 100% accuracy on the training data (α_{train}) after 30 epochs, but the maximum accuracy on the testing data ($\alpha_{\text{test}} = 80\%$) was reached after 11 epochs, suggesting potential overfitting (Figure 6). The model trained after 11 epochs was adopted for the future CDW classification.

2.4.4. Model Evaluation Metrics

To evaluate the performance of our multi-class classification models, we primarily utilize accuracy and the weighted F-score.

Let P_c^{true} be the number of true positives for class c, N_c^{true} the true negatives, P_c^{false} the false

Table 4: Architecture of the CNN models; the individual layers were implemented in the Tensorflow Keras v.2.10.0 Python package, the *layers* class.

Layer	Keras class	Purpose
Convolutional layer (32 filters, size 3×3)	*Conv2D(32, (3, 3), 1, activation='relu', input_shape=(200, 200, 3))*	Extract features from the input images
Maximum pooling layer (2×2 pool)	*MaxPooling2D()*	Downsample the feature maps from the previous layer
Convolutional layer (64 filters, size 3×3)	*Conv2D(64, (3, 3), 1, activation='relu')*	Extract features from the previous layer
Maximum pooling layer (2×2 pool)	*MaxPooling2D()*	Downsample the feature maps from the previous layer
Convolutional layer (32 filters, size 3×3)	*Conv2D(32, (3, 3), 1, activation='relu')*	Extract features from the previous layer
Flattening layer	*Flatten()*	Flattens the 2D feature map into a 1D array
Fully connected layer (256 neurons)	*Dense(256, activation='relu')*	Take the flattened vector from the previous layer as input
Output layer (4 neurons)	*Dense(4)*	Values of individual neurons represent probabilities that the input belongs to each of the possible classes

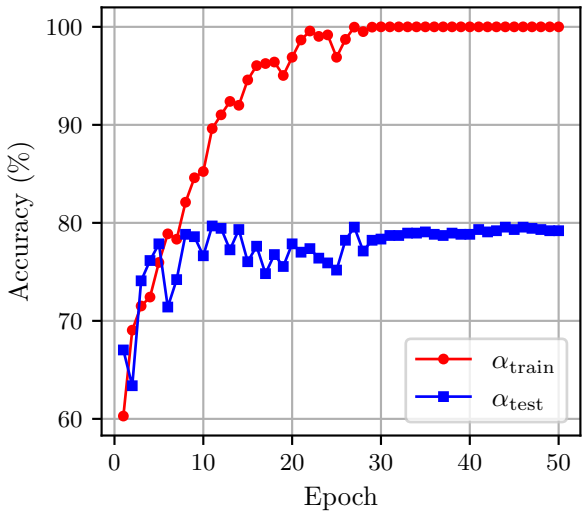

Figure 6: Training and testing accuracy as a function of epoch recorded during CNN training.

positives, and N_c^{false} the false negatives. Accuracy, denoted by α, measures the proportion of all correct predictions across all four classes:

$$\alpha = \frac{\sum_{c=1}^{4} P_c^{\text{true}} + N_c^{\text{true}}}{\sum_{c=1}^{4} P_c^{\text{true}} + N_c^{\text{true}} + P_c^{\text{false}} + N_c^{\text{false}}}. \tag{6}$$

The precision P_c and recall R_c for each class are respectively defined as:

$$P_c = \frac{P_c^{\text{true}}}{P_c^{\text{true}} + P_c^{\text{false}}} \quad \text{and} \quad R_c = \frac{P_c^{\text{true}}}{P_c^{\text{true}} + N_c^{\text{false}}} \tag{7}$$

The F-score for class c, denoted as F_c, offers a balance between P_c and R_c. It is described as the harmonic mean of P_c and R_c:

$$F_c = \frac{2P_cR_c}{P_c + R_c} \tag{8}$$

For our multi-class problem, the weighted F-score, F_{weighted}, is calculated by averaging the F-score of each class, weighted by the proportion of samples from that class:

$$F_{\text{weighted}} = \sum_{c=1}^{4} w_c F_c \tag{9}$$

where w_c denotes the weight (proportion of samples) for the c^{th} class.

We employ both α and F_{weighted} in this study to evaluate the performance of our classifiers, providing a comprehensive view of their efficacy, especially in light of the minor class imbalance present in our dataset.

3. Results and discussion

The performance of individual classifiers is represented through confusion matrices (Figure 7), alongside the results of "manual" classification. This manual classification was accomplished using an online survey[3] by five experts on building materials from the Faculty of Civil Engineering, Czech Technical University in Prague.

While accuracy provides a general measure of correctness, the weighted F-score offers a more balanced measure between precision (how many selected items are relevant) and recall (how many relevant items are selected). For instance, GB and MLP classifiers achieved an accuracy of 82.5% with F-scores of 82.4%, indicating a harmonious balance between precision and recall. The CNN classifier achieved an accuracy of 82.1% and an F-score of 82.3%, further demonstrating the model's consistent performance. In comparison, human experts achieved an accuracy of 87.2% and an F-score of 87.5%, outperforming the machine classifiers slightly.

Both machine-learning classifiers and human experts had difficulties distinguishing between image samples of AAC, asphalt, and concrete. This demonstrates the inherent difficulty in differentiating these materials visually, particularly when they share similar characteristics like a grayish color and texture. In contrast, ceramics (bricks, roof tiles, etc.) were recognized with an impressive accuracy of over 96% by both groups. A potential enhancement to the classification process could be the integration of a basic weight measurement device. Given the significant differences in density between the grayish materials, weight can be a distinguishing factor. Moreover, if a dual-camera setup were employed, the segmentation technique would permit volume estimation from visual data, further refining the differentiation process.

Despite the commendable performance of human experts, there are inherent limitations to relying on manual sorting. Prolonged concentration can lead to lapses in attention, impacting the consistency of the sorting process (Firestone, 2020). Furthermore, machine classifiers, especially when deployed on standard office computers, can process samples at a rate that outpaces human capability by orders of magnitude.

[3] https://rm.fsv.cvut.cz/cdw/

In recent literature, Davis et al. (2021) reported accuracy levels between 80% and 97% for the CNN-based classification of general waste. Their categories included paper, glass, plastic, metal, cardboard, and non-recyclables. Although their work achieved an accuracy of up to 95.7% for CDW, it's crucial to note that the objects they classified had more distinct shapes than the CDW fragments. Xiao et al. (2019) reported a perfect accuracy of 100% in their classification of CDW on a conveyor belt. They employed a high-cost near-infrared hyperspectral camera and a dataset with distinct categories like foam, plastic, brick, concrete, and wood. Introducing more challenging materials such as asphalt conglomerates or AAC, often found in CDW, could potentially reduce this high accuracy even with advanced hardware.

A study on the performance of the individual classifiers in terms of speed and accuracy is presented as a function of subset size in Figure 8. As larger subsets contained more information, the accuracy of models increased. This phenomenon was most significant in the case of CNN, for which the image subsets had to be rescaled to 200×200 px to have the same size as images used for training. Similar findings were reported by Dimitrov and Golparvar-Fard (2014), who developed a system for vision-based material recognition and monitoring of construction progress, employing the support vector machine (SVM) classifier (Cortes and Vapnik, 1995).

In our study, the GB and MLP models that utilized feature extraction, exhibited similar speed and accuracy, both superior to CNN, especially for small subsets. Unlike CNN, both models approached their maximum accuracies at approximately 150×150 px subset size. The classification speed of GB and MLP classifiers, including feature extraction, was about 15× higher compared to CNN.

The practical demonstration of the image subset classification is provided in Figure 9. Here, the randomly selected CDW fragments from the testing dataset were localized using the Rembg[4] Python package based on the U^2-Net deep neural network (Qin et al., 2020). An auxiliary script was designed to extract image subsets from the unmasked regions. The accuracy of the CNN classifier was compromised by the small size (135×135 px) subsets placed over the region of interest; however, even despite this shortcoming, even the CNN classified the fragments correctly

[4] https://github.com/danielgatis/rembg

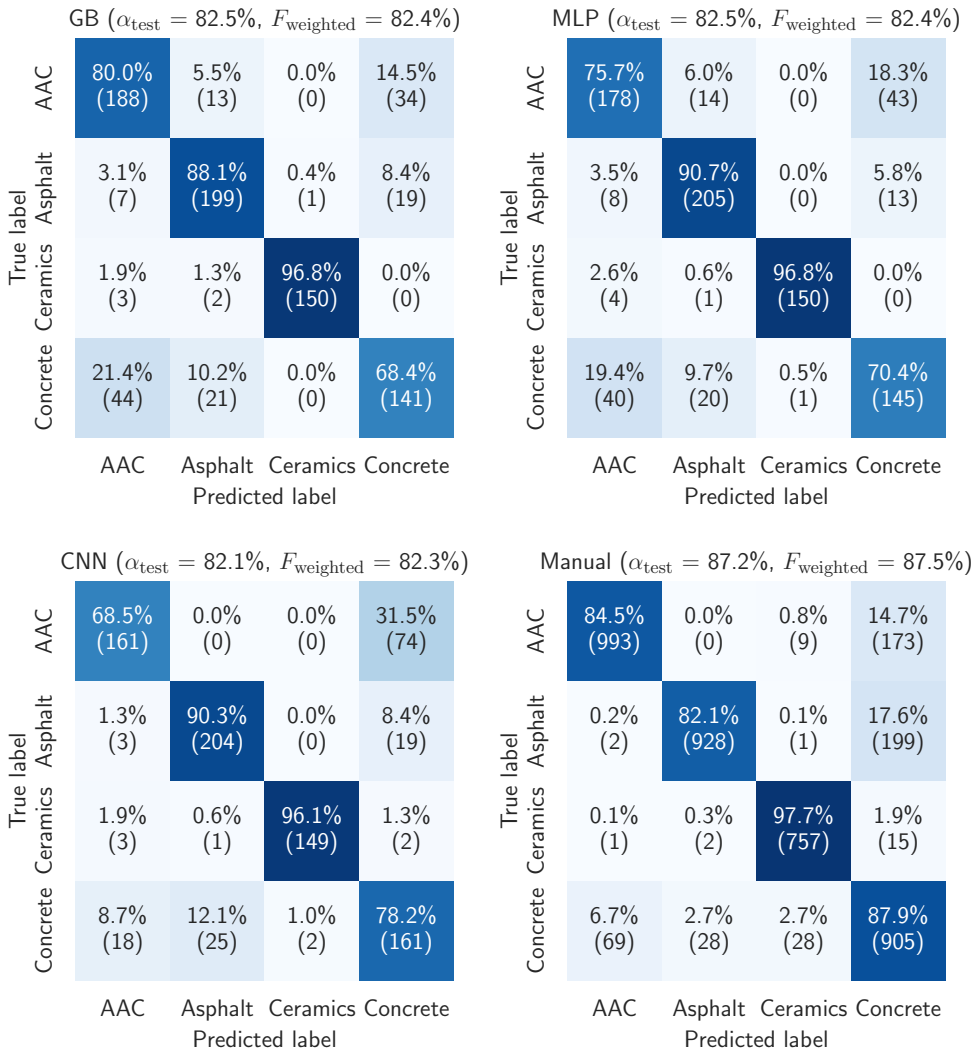

Figure 7: Confusion matrices for different classifiers and comparison of their performance with manual classification done by five experts on building materials from the FCE CTU in Prague.

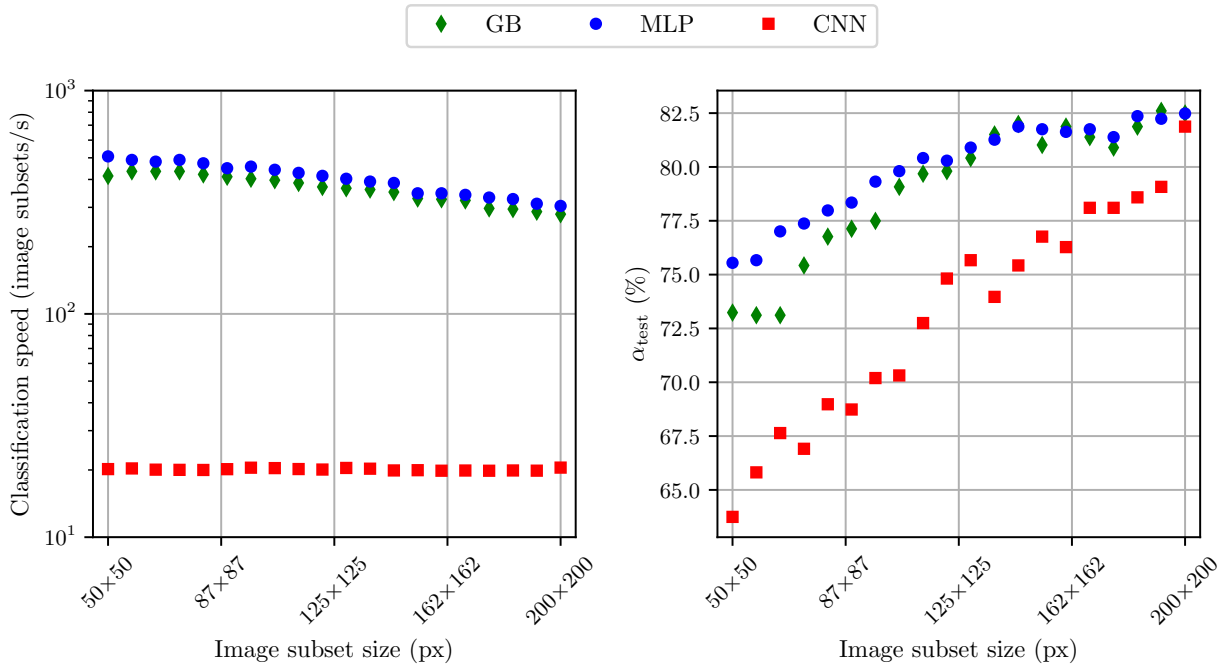

Figure 8: Speed (left) and accuracy (right) reached by individual classifiers on the validation (testing) datasets for different sizes of image subsets that were extracted by cropping the redundant portion of the images.

with high confidence. Nearly 100% confidence was reached by the GB and MLP classifiers.

This demonstration shows that the accuracy reached for individual subsets is improved by placing a higher number of these over the samples. The accuracy was tested on a comprehensive dataset containing 2664 images of CDW framents (Nežerka et al., 2023); the summary of reached accuracies for individual classifiers is provided in Table 5. Classification of several samples per a CDW fragment led to overall accuracy ranging between 85.9% (CNN) and 92.3% (GB), reaching the accuracy reported by other authors dealing with the classification of clean building materials. In a study by Mahami et al. (2020), the authors managed to classify eleven construction materials using CNN (VGG16 network (Simonyan and Zisserman, 2014)) and reached up to 97.35% accuracy, yet, their dataset did not contain contaminated materials having similar textures, such as fragments of AAC and concrete in our study.

Table 5: Accuracy of different classifiers when recognizing whole CDW fragments by classifying several (>4) 200×200 image subsets with a 70 px overlap (Figure 10).

Classifier	AAC (582 images)	Asphalt (741 images)	Ceramics (572 images)	Concrete (769 images)	Complete dataset (2664 images)
GB	86.9%	93.9%	99.1%	89.7%	92.3%
MLP	89.4%	93.8%	98.4%	85.2%	91.3%
CNN	56.7%	97.2%	99.0%	87.5%	85.9%

Our models, especially the Gradient Boosting and Multi-Layer Perceptron classifiers, demonstrated competitive performance when compared to previous studies, as summarized in Table 6. Notably, while our dataset size was comprehensive, the nature of our CDW images, which included contaminated materials with similar textures, made the classification task more challenging.

It should be noted that all the images for both training and testing datasets were taken using the same camera and similar conditions, which can compromise the robustness of the classification models. The goal of this proof-of-the-concept study is to demonstrate the capabilities of the proposed low-cost lightweight procedures that could be implemented in CDW sorting and recycling plants for CDW recognition on conveyor belts. For particular industrial applications, new site-specific training datasets should be acquired, optimally involving auxiliary data (weight, acoustic emissions, etc.) from other sensors. Fusion of RGB cameras with different sensors could signif-

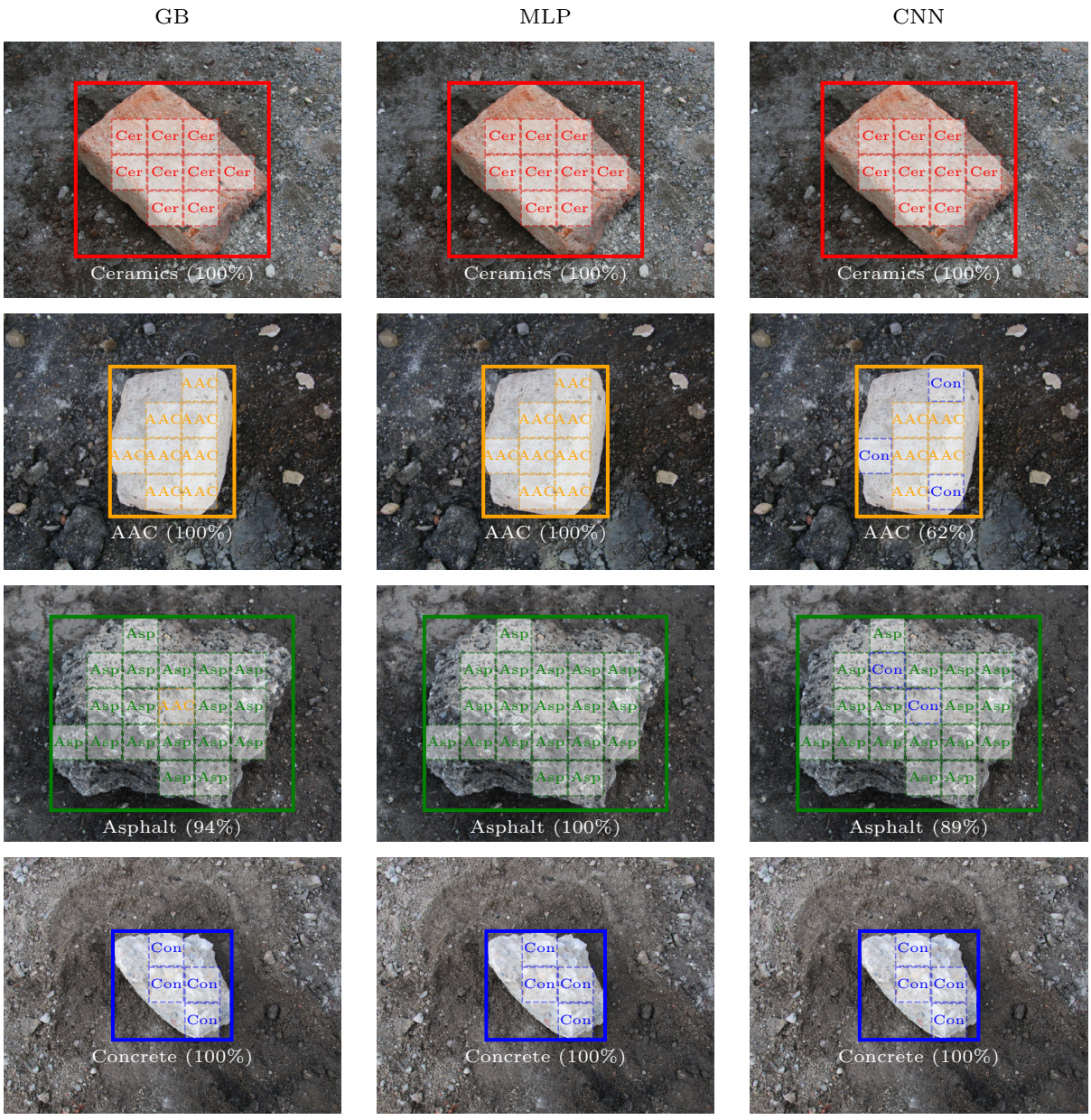

Figure 9: Localization of whole CDW fragments and their classification based on texture recognition using different classifiers; the size of image subsets 135×135 px.

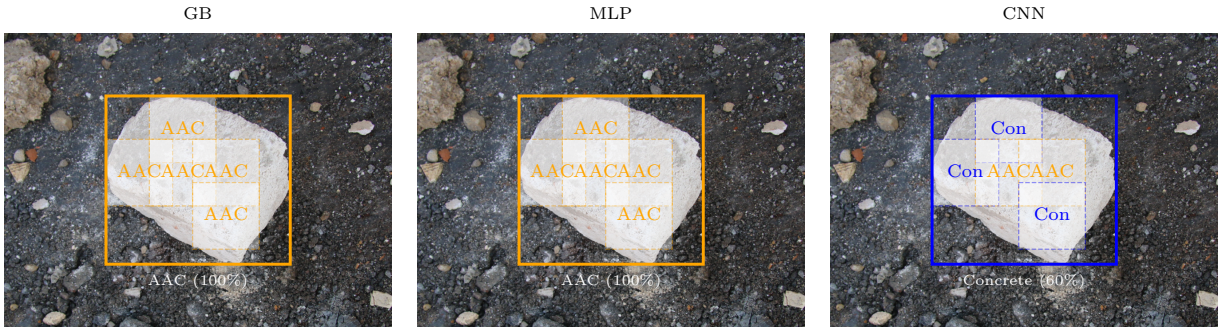

Figure 10: A typical misclassification of AAC fragments by CNN during a comprehensive validation of the classification algorithms; size of image subsets 200×200 px with a 70 px overlap.

Table 6: Comparison of the current study with previous significant works focused on machine-learning-based recognition of construction materials in terms of model performance, data type, and dataset size.

Reference	Model	Accuracy	Dataset type and size	Dataset size
This study (GB)	GB	92.3%	CDW images	2664
This study (MLP)	MLP	91.3%	CDW images	2664
This study (CNN)	CNN	85.9%	CDW images	2664
Davis et al. (2021)	CNN	80-97%	Images of conatiners with bulk CDW	2283
Xiao et al. (2019)	CNN	100%	Hyperspectral images of very diverse materials	250
Dimitrov and Golparvar-Fard (2014)	SVM	Up to 97.1%	Point cloud patches (images of construction surfaces)	3740
Mahami et al. (2020)	CNN (VGG16)	97.35%	Images of clean very diverse materials	1231
Yuan et al. (2021)	BD-P model	90.2%	Bulk density (truck loads)	4.27 mil.
Hoong et al. (2020)	CNN (Custom ResNet34)	97%	Images of recycled aggregates	36000
Lin et al. (2022)	CNN (CVGGNet-16)	76.6%	Images of diverse clean bulk materials	2836 (bofore augmentation)

icantly increase the accuracy, especially in the case of lightweight AAC which is often confused with fragments of concrete that also have a fine texture and grayish color.

3.1. Application procedure

Our developed machine-learning-assisted method for CDW fragment recognition is designed for easy integration into existing CDW sorting systems. Here, we outline the potential application procedure:

1. **Image Acquisition**: Using high-resolution cameras, images of CDW fragments on conveyor belts or sorting platforms are captured. Ideally, this would be integrated into a continuous flow system where CDW moves along a conveyor.
2. **Preprocessing**: The captured images undergo preprocessing, which may include cleaning using air-flow or other mechanisms to enhance clarity, and then they are fed into the model.
3. **Density Estimation**: For individual fragments on the conveyor belt, a weight measurement system can be integrated to estimate the density of each fragment. This can assist in further refining the classification, especially for fragments with similar appearances but different densities (e.g., AAC and concrete).
4. **Classification**: The preprocessed images are classified in real-time using a trained model. The model identifies the type of CDW fragment and can potentially direct its sorting into appropriate bins or sections.
5. **Post-processing**: Based on classifications, automated mechanisms or manual laborers can be directed to ensure correct sorting or further refinement.
6. **Feedback Loop**: The system can be designed to continuously learn from any misclassifications through a feedback mechanism, enhancing accuracy over time.

This proposed application procedure is modular and can be customized based on the specific requirements of the CDW sorting facility, available resources, and desired accuracy levels.

4. Conclusion

Proper sorting of construction and demolition waste (CDW) fragments is essential for its further valorization. In this study, we demonstrated the potential of machine-learning models for the

recognition and classification of CDW fragments using computer vision-based algorithms. The approach was tested on four types of CDW material fragments commonly found in mixed debris from demolition sites: aerated autoclaved concrete (AAC), asphalt conglomerates, ceramics (roof tiles and bricks), and concrete fragments. For that purpose, we examined three machine-learning classification models, gradient boosting (GB), multi-layer perception (MLP), and convolutional neural network (CNN).

In contrast to CNN, having the 200×200×3 px RGB images as its input, GB and MLP were trained on classifying the CDW texture based on four extracted features: (i) mean intensity, (ii) mean intensity of the red color channel, (iii) Shannon entropy, and (iv) mean intensity gradient, reducing the input space from $D = 120,000$ to $D = 4$. In the case of CNN, the feature extraction was accomplished using convolutional layers. The GB and MLP classifiers outperformed CNN not only in terms of speed (for a single image subset ∼300 s^{-1} vs. ∼20 s^{-1}), but also accuracy, especially when classifying images of sizes below 200×200 px, on which the models were trained.

Despite the high similarity of the recognized textures and contamination of the CDW fragments with dust, the examined classifiers exhibited accuracy over 82.1% for 200×200 px image subsets, slightly below the average accuracy reached by experts on building materials (87.2%). The accuracy reached up to 92.3% (GB) when classifying the whole fragments by placing several subsets over the samples. The lowest overall accuracy was reached when using CNN because the model often misclassified AAC for concrete. All the models were most accurate when classifying fragments of ceramics (98.4–99.1%) because of their distinct reddish color.

However, this study comes with certain limitations. All images, both for training and testing datasets, were acquired under similar conditions using the same camera, which might affect the robustness of the classifiers in more varied settings. Moreover, while the study showcases the capabilities of low-cost procedures for CDW recognition, it underscores the need for acquiring new site-specific training datasets for specific industrial applications; optimally on a conveyor belt. The integration of additional sensors or data sources could further enhance accuracy and reliability.

The links to image datasets, computer codes, and pre-trained models used in this study are open and are provided as supplementary material. We believe that the findings can promote the

developments in robotics-assisted sorting of CDW fragments, enabling its efficient use in the production of new materials and products and reduction of the environmental burden associated with CDW disposal.

Funding. This work was supported by the European Union's Horizon Europe Framework Programme (call HORIZON-CL4-2021-TWIN-TRANSITION-01-11) under grant agreement No. 101058580, project RECONMATIC (Automated solutions for sustainable and circular construction and demolition waste management), the Technology Agency of the Czech Republic, grant agreement No. S03010302 (Development of efficient tools to minimize production of construction and demolition waste, its monitoring and reuse), and the Czech Technical University in Prague, grant agreement No. SGS23/004/OHK1/1T/11 (Development and application of digitized and automated tools for multi-purpose applications in the construction sector).

References

J. Antoš, V. Nežerka, and M. Somr. Assessment of 2D-DIC stochastic patterns. *Acta Polytechnica CTU Proceedings*, 13:1–10, 2017. doi: 10.14311/app.2017.13.0001.

G. L. F. Benachio, M. do Carmo Duarte Freitas, and S. F. Tavares. Circular economy in the construction industry: A systematic literature review. *Journal of Cleaner Production*, 260: 121046, 2020. doi: 10.1016/j.jclepro.2020.121046.

F. Bosché, M. Ahmed, Y. Turkan, C. T. Haas, and R. Haas. The value of integrating scan-to-BIM and scan-vs-BIM techniques for construction monitoring using laser scanning and BIM: The case of cylindrical MEP components. *Automation in Construction*, 49:201–213, 2015. doi: 10.1016/j.autcon.2014.05.014.

A. Braun and A. Borrmann. Combining inverse photogrammetry and BIM for automated labeling of construction site images for machine learning. *Automation in Construction*, 106:102879, 2019. doi: 10.1016/j.autcon.2019.102879.

C. Cortes and V. Vapnik. Support-vector networks. *Machine Learning*, 20:273–297, 1995. doi: 10.1007/bf00994018.

A. Darko, A. P. Chan, M. A. Adabre, D. J. Edwards, M. R. Hosseini, and E. E. Ameyaw. Artificial intelligence in the AEC industry: Scientometric analysis and visualization of research activities. *Automation in Construction*, 112:103081, 2020. doi: 10.1016/j.autcon.2020.103081.

P. Davis, F. Aziz, M. T. Newaz, W. Sher, and L. Simon. The classification of construction waste material using a deep convolutional neural network. *Automation in Construction*, 122:103481, 2021. doi: 10.1016/j.autcon.2020.103481.

F. N. M. de Sousa Filho, V. G. Pereira de Sá, and E. Brigatti. Entropy estimation in bidimensional sequences. *Physical Review E*, 105:054116, 2022. doi: 10.1103/physreve.105.054116.

A. Dimitrov and M. Golparvar-Fard. Vision-based material recognition for automated monitoring of construction progress and generating building information modeling from unordered site image collections. *Advanced Engineering Informatics*, 28:37–49, 2014. doi: 10.1016/j.aei.2013.11.002.

Z. Dong, J. Chen, and W. Lu. Computer vision to recognize construction waste compositions: A novel boundary-aware transformer (BAT) model. *Journal of Environmental Management*, 305:114405, 2022. doi: 10.1016/j.jenvman.2021.114405.

C. Firestone. Performance vs. competence in human-machine comparisons. *Proceedings of the National Academy of Sciences*, 117:26562–26571, 2020. doi: 10.1073/pnas.1905334117.

J. H. Friedman. Greedy function approximation: A gradient boosting machine. *The Annals of Statistics*, 29:1189–1232, 2001. doi: 10.1214/aos/1013203451.

J. H. Friedman. Stochastic gradient boosting. *Computational Statistics & Data Analysis*, 38:367–378, 2002. doi: 10.1016/s0167-9473(01)00065-2.

A. Géron. *Hands-on machine learning with Scikit-Learn, Keras, and TensorFlow*. O'Reilly Media, Inc., 2022.

S. P. Gundupalli, S. Hait, and A. Thakur. A review on automated sorting of source-separated municipal solid waste for recycling. *Waste Management*, 60:56–74, 2017. doi: 10.1016/j.wasman.2016.09.015.

K. K. Han and M. Golparvar-Fard. Appearance-based material classification for monitoring of operation-level construction progress using 4d BIM and site photologs. *Automation in Construction*, 53:44–57, 2015. doi: 10.1016/j.autcon.2015.02.007.

T. Hastie, R. Tibshirani, and J. Friedman. Boosting and additive trees. In *The Elements of Statistical Learning*, pages 337–387. 2008. doi: 10.1007/978-0-387-84858-7_10.

G. E. Hinton, S. Osindero, and Y.-W. Teh. A fast learning algorithm for deep belief nets. *Neural Computation*, 18:1527–1554, 2006. doi: 10.1162/neco.2006.18.7.1527.

R. Hlůžek, J. Trejbal, V. Nežerka, P. Demo, Z. Prošek, and P. Tesárek. Improvement of bonding between synthetic fibers and a cementitious matrix using recycled concrete powder and plasma treatment: from a single fiber to FRC. *European Journal of Environmental and Civil Engineering*, 26:3880–3897, 2020. doi: 10.1080/19648189.2020.1824821.

S. Y.-C. Ho, T.-W. Chien, M.-L. Lin, and K.-T. Tsai. An app for predicting patient dementia classes using convolutional neural networks (CNN) and artificial neural networks (ANN): Comparison of prediction accuracy in microsoft excel. *Medicine*, 102:e32670, 2023. doi: 10.1097/md.0000000000032670.

J. D. L. H. Hoong, J. Lux, P.-Y. Mahieux, P. Turcry, and A. Aït-Mokhtar. Determination of the composition of recycled aggregates using a deep learning-based image analysis. *Automation in Construction*, 116:103204, 2020. doi: 10.1016/j.autcon.2020.103204.

T. Joensuu, H. Edelman, and A. Saari. Circular economy practices in the built environment. *Journal of Cleaner Production*, 276:124215, 2020. doi: 10.1016/j.jclepro.2020.124215.

D. P. Kingma and J. Ba. Adam: A method for stochastic optimization. In Y. Bengio and Y. LeCun, editors, *3rd International Conference on Learning Representations, ICLR 2015, San Diego, CA,*

USA, May 7-9, 2015, Conference Track Proceedings, 2015. URL http://arxiv.org/abs/1412.6980.

A. Krizhevsky, I. Sutskever, and G. E. Hinton. ImageNet classification with deep convolutional neural networks. *Communications of the ACM*, 60:84–90, 2017. doi: 10.1145/3065386.

Y. Ku, J. Yang, H. Fang, W. Xiao, and J. Zhuang. Deep learning of grasping detection for a robot used in sorting construction and demolition waste. *Journal of Material Cycles and Waste Management*, 23:84–95, 2020. doi: 10.1007/s10163-020-01098-z.

Y. LeCun, Y. Bengio, and G. Hinton. Deep learning. *Nature*, 521:436–444, 2015. doi: 10.1038/nature14539.

S. Liang and Y. Gu. A deep convolutional neural network to simultaneously localize and recognize waste types in images. *Waste Management*, 126:247–257, 2021. doi: 10.1016/j.wasman.2021.03.017.

K. Lin, T. Zhou, X. Gao, Z. Li, H. Duan, H. Wu, G. Lu, and Y. Zhao. Deep convolutional neural networks for construction and demolition waste classification: VGGNet structures, cyclical learning rate, and knowledge transfer. *Journal of Environmental Management*, 318:115501, 2022. doi: 10.1016/j.jenvman.2022.115501.

W. Lu and J. Chen. Computer vision for solid waste sorting: A critical review of academic research. *Waste Management*, 142:29–43, 2022. doi: 10.1016/j.wasman.2022.02.009.

H. Mahami, N. Ghassemi, M. T. Darbandy, A. Shoeibi, S. Hussain, F. Nasirzadeh, R. Alizadehsani, D. Nahavandi, A. Khosravi, and S. Nahavandi. Material recognition for automated progress monitoring using deep learning methods, 2020.

A. Mahpour. Prioritizing barriers to adopt circular economy in construction and demolition waste management. *Resources, Conservation and Recycling*, 134:216–227, 2018. doi: 10.1016/j.resconrec.2018.01.026.

K. P. Murphy. *Probabilistic machine learning: an introduction*. MIT press, 2022.

M. H. A. Nasir, A. Genovese, A. A. Acquaye, S. Koh, and F. Yamoah. Comparing linear and circular supply chains: A case study from the construction industry. *International Journal of Production Economics*, 183:443–457, 2017. doi: 10.1016/j.ijpe.2016.06.008.

V. Nežerka, J. Trejbal, and T. Zbíral. Dataset of construction and demolition waste images: aerated autoclaved concrete (AAC), asphalt, ceramics, and concrete, Feb. 2023.

V. Nežerka and J. Trejbal. Assessment of aggregate-bitumen coverage using entropy-based image segmentation. *Road Materials and Pavement Design*, pages 1–12, 2019. doi: 10.1080/14680629.2019.1605304.

V. Nežerka, Z. Prošek, J. Trejbal, J. Pešta, J. Ferriz-Papi, and P. Tesárek. Recycling of fines from waste concrete: Development of lightweight masonry blocks and assessment of their environmental benefits. *Journal of Cleaner Production*, 385:135711, 2023. doi: 10.1016/j.jclepro.2022.135711.

M. S. Nixon and A. S. Aguado. Image processing. In *Feature Extraction and Image Processing for Computer Vision*, pages 83–139. Elsevier, 2020. doi: 10.1016/b978-0-12-814976-8.00003-8.

M. Norouzi, M. Chàfer, L. F. Cabeza, L. Jiménez, and D. Boer. Circular economy in the building and construction sector: A scientific evolution analysis. *Journal of Building Engineering*, 44:102704, 2021. doi: 10.1016/j.jobe.2021.102704.

B. I. Oluleye, D. W. Chan, A. B. Saka, and T. O. Olawumi. Circular economy research on building construction and demolition waste: A review of current trends and future research directions. *Journal of Cleaner Production*, 357:131927, 2022. doi: 10.1016/j.jclepro.2022.131927.

K. Özkan, S. Ergin, Ş. Işık, and İ. Işıklı. A new classification scheme of plastic wastes based upon recycling labels. *Waste Management*, 35:29–35, 2015. doi: 10.1016/j.wasman.2014.09.030.

B. Pan, Z. Lu, and H. Xie. Mean intensity gradient: An effective global parameter for quality assessment of the speckle patterns used in digital image correlation. *Optics and Lasers in Engineering*, 48:469–477, 2010. doi: 10.1016/j.optlaseng.2009.08.010.

S. M. Piryonesi and T. E. El-Diraby. Using machine learning to examine impact of type of performance indicator on flexible pavement deterioration modeling. *Journal of Infrastructure Systems*, 27:04021005, 2021. doi: 10.1061/(asce)is.1943-555x.0000602.

Z. Prošek, J. Trejbal, V. Nežerka, V. Goliáš, M. Faltus, and P. Tesárek. Recovery of residual anhydrous clinker in finely ground recycled concrete. *Resources, Conservation and Recycling*, 155:104640, 2020. doi: 10.1016/j.resconrec.2019.104640.

C. K. Purchase, D. M. A. Zulayq, B. T. O'Brien, M. J. Kowalewski, A. Berenjian, A. H. Tarighaleslami, and M. Seifan. Circular economy of construction and demolition waste: A literature review on lessons, challenges, and benefits. *Materials*, 15:76, 2021. doi: 10.3390/ma15010076.

X. Qin, Z. Zhang, C. Huang, M. Dehghan, O. Zaiane, and M. Jagersand. U2-net: Going deeper with nested u-structure for salient object detection. *Pattern Recognition*, 106:107404, 2020.

D. E. Rumelhart, G. E. Hinton, and R. J. Williams. Learning representations by back-propagating errors. *Nature*, 323:533–536, 1986. doi: 10.1038/323533a0.

S. L. Salzberg. C4.5: Programs for machine learning by j. ross quinlan. morgan kaufmann publishers, inc., 1993. *Machine Learning*, 16:235–240, 1994. doi: 10.1007/bf00993309.

C. E. Shannon. A mathematical theory of communication. *Bell System Technical Journal*, 27: 623–656, 1948. doi: 10.1002/j.1538-7305.1948.tb00917.x.

K. Simonyan and A. Zisserman. Very deep convolutional networks for large-scale image recognition, 2014.

H. Son, C. Kim, and C. Kim. Automated color model-based concrete detection in construction-site images by using machine learning algorithms. *Journal of Computing in Civil Engineering*, 26: 421–433, 2012. doi: 10.1061/(asce)cp.1943-5487.0000141.

Y. Su. Multi-agent evolutionary game in the recycling utilization of construction waste. *Science of The Total Environment*, 738:139826, 2020. doi: 10.1016/j.scitotenv.2020.139826.

J. Valentin, J. Trejbal, V. Nežerka, T. Valentová, and M. Faltus. Characterization of quarry dusts and industrial by-products as potential substitutes for traditional fillers and their impact on water susceptibility of asphalt concrete. *Construction and Building Materials*, 301:124294, 2021. doi: 10.1016/j.conbuildmat.2021.124294.

T. Vincent, M. Guy, P. Louis-César, B. Jean-François, and M. Richard. Physical process to sort construction and demolition waste (c&dw) fines components using process water. *Waste Management*, 143:125–134, 2022. doi: 10.1016/j.wasman.2022.02.012.

Z. Wang, H. Li, and X. Zhang. Construction waste recycling robot for nails and screws: Computer vision technology and neural network approach. *Automation in Construction*, 97:220–228, 2019a. doi: 10.1016/j.autcon.2018.11.009.

Z. Wang, B. Peng, Y. Huang, and G. Sun. Classification for plastic bottles recycling based on image recognition. *Waste Management*, 88:170–181, 2019b. doi: 10.1016/j.wasman.2019.03.032.

Z. Wang, H. Li, and X. Yang. Vision-based robotic system for on-site construction and demolition waste sorting and recycling. *Journal of Building Engineering*, 32:101769, 2020. doi: 10.1016/j.jobe.2020.101769.

Y. Wu, J. P. Noonan, and S. Agaian. A novel information entropy based randomness test for image encryption. In *2011 IEEE International Conference on Systems, Man, and Cybernetics*. IEEE, 2011. doi: 10.1109/icsmc.2011.6084076.

Y. Wu, Y. Zhou, G. Saveriades, S. Agaian, J. P. Noonan, and P. Natarajan. Local shannon entropy measure with statistical tests for image randomness. *Information Sciences*, 222:323–342, 2013. doi: 10.1016/j.ins.2012.07.049.

W. Xiao, J. Yang, H. Fang, J. Zhuang, and Y. Ku. Development of online classification system for construction waste based on industrial camera and hyperspectral camera. *PLOS ONE*, 14: e0208706, 2019. doi: 10.1371/journal.pone.0208706.

W. Xiao, J. Yang, H. Fang, J. Zhuang, and Y. Ku. Classifying construction and demolition waste by combining spatial and spectral features. *Proceedings of the Institution of Civil Engineers—Waste and Resource Management*, 173:79–90, 2020. doi: 10.1680/jwarm.20.00008.

J. Yang, Z. Zeng, K. Wang, H. Zou, and L. Xie. GarbageNet: A unified learning framework for robust garbage classification. *IEEE Transactions on Artificial Intelligence*, 2:372–380, 2021. doi: 10.1109/tai.2021.3081055.

L. Yuan, J. Guo, and Q. Wang. Automatic classification of common building materials from 3d terrestrial laser scan data. *Automation in Construction*, 110:103017, 2020. doi: 10.1016/j.autcon.2019.103017.

L. Yuan, W. Lu, and F. Xue. Estimation of construction waste composition based on bulk density: A big data-probability (BD-p) model. *Journal of Environmental Management*, 292:112822, 2021. doi: 10.1016/j.jenvman.2021.112822.

T. Zbíral and V. Nežerka. Python codes for machine-learning-based classification of construction and demolition waste fragments, Feb. 2023.

L. Zheng, H. Wu, H. Zhang, H. Duan, J. Wang, W. Jiang, B. Dong, G. Liu, J. Zuo, and Q. Song. Characterizing the generation and flows of construction and demolition waste in China. *Construction and Building Materials*, 136:405–413, 2017. doi: 10.1016/j.conbuildmat.2017.01.055.

S. Zhou, Q. Chen, and X. Wang. Convolutional deep networks for visual data classification. *Neural Processing Letters*, 38:17–27, 2012. doi: 10.1007/s11063-012-9260-y.

Z.-H. Zhou. Decision trees. In *Machine Learning*, pages 79–102. Springer Singapore, 2021. doi: 10.1007/978-981-15-1967-3_4.

Z. Zhu and I. Brilakis. Parameter optimization for automated concrete detection in image data. *Automation in Construction*, 19:944–953, 2010. doi: 10.1016/j.autcon.2010.06.008.